

Response to referee #1 (in RC2)

RC: This paper presents a new method for retrieving the ice particle number concentration  $N_i$  for glaciated clouds, which should be useful for understanding aerosol interactions with ice clouds and the contribution of homogeneous vs. heterogeneous ice nucleation in cirrus clouds. A satellite remote sensing scheme for  $N_i$  is needed since field campaigns cannot adequately inform us how  $N_i$  varies with latitude and the seasons. The paper is well organized and well written, and usually cites the relevant literature. The quality of the figures is good. The methods developed in Sec. 5 for testing the retrieval are especially creative and effective.

AR: We are thankful to the referee for all the useful comments that greatly helped us to improve the quality and clarify of this study. In particular concerning the influence of the PSD shape assumptions, the use of 2D-S data and the consistency between the analyses of  $N_i$  climatologies presented in the 2 papers of this study. Detailed responses to each comment are provided below.

---

RC: A critical limitation of the retrieval algorithm is the use of a normalized universal ice particle size distribution, or PSD (Delanoë et al., 2005), where it is assumed that all PSD in nature conform to this normalized PSD shape. This normalized PSD is based on a four-parameter gamma function (Eq. 4) where parameters  $N_0$  and  $k$  can be deduced through their link with other operationally retrieved properties (IWC and  $N_0^*$ ) while PSD parameters  $\alpha$  and  $\beta$  need to be fixed as constants. This is of little consequence regarding  $\beta$ , which affects the largest ice particles having the lowest concentrations. But this is of major consequence regarding  $\alpha$ , which strongly influences the smallest ice particles that govern  $N_i$ . This is not mentioned in the paper. The small end of the PSD is sensitive to the rate of ice nucleation which is sensitive to the cloud updraft  $w$  (with higher  $w$  making  $\alpha$  more negative, and  $N_i$  higher), as well as the aggregation rate that removes smaller ice particles having higher concentration (Herzogh and Hobbs, 1985, QJRMS; Mitchell, 1991, JAS). Thus, some discussion on this topic is warranted, especially on the errors that may result from “non-standard” conditions where atypical updrafts are common (such as over steep orography).

AR: We thank the referee for pointing out the need for further discussion regarding the impact of non-retrieved shape parameters of the size distributions ( $\alpha$  and  $\beta$ ). We completely agree that this was lacking in the original manuscript.

DARDAR unfortunately does not rigorously account for these uncertainties in its operational retrievals, as they are only represented by additional fixed errors considered on the lidar and radar measurements. More rigorous techniques exist to propagate uncertainties on  $\alpha$  and  $\beta$  through the optimal estimation scheme but they would be too time consuming for an operational algorithm based on active instruments. However, the variability of these two parameters and the subsequent impact on DARDAR has been thoroughly discussed in Delanoë et al. [2014]. It can be noted that, as a result of this study, a revised version of the PSD parameterization has been proposed (notably with a less negative  $\alpha$ , leading to less small ice crystals and a lower  $N_i$ ) but is not yet implemented in the operational product. The referee is therefore absolutely correct in saying that the fixed  $\alpha$  and  $\beta$  parameters constitute a strong limitation to our current method that should be further highlighted. These points are now discussed in Sec. 3.1 and in Appendix

A3 of the revised manuscript and are supported by additional figures in the supplementary materials (see Fig. S3).

The impact of the choice of  $\alpha$  and  $\beta$  on the PSD shape is clearly shown in the upper panel of Fig. S3, and the subsequent impact on  $N_i$  because of straying from the selected values ( $\alpha = -3$  and  $\beta = -1$ ) is quantified in the lower figure. In order to propose a range of realistic shape parameters, values extracted by Delanoë et al. [2014] from individual in situ campaigns are used (color code in upper figure and shapes in the lower figure). IWC and  $N_0^*$  values representative of 3 temperature bins are selected, although it should be kept in mind that each couple of coefficients from the D14 campaigns can realistically applied to only one of these temperature ranges. In agreement with the referee's comment, it can be observed that one D14 campaign displays a more negative  $\alpha$ , namely the "subvisible" campaign, which corresponds to cirrus measured at temperatures between  $-80$  to  $-60^\circ\text{C}$  during CRYSTAL-FACE (Cirrus Regional Study of Tropical Anvils and Cirrus-Layers-Florida Area Cirrus Experiment). We recognize that this analysis remains preliminary but it should still allow to provide rough estimates of the uncertainties on  $N_i^{5\mu\text{m}}$ ,  $N_i^{25\mu\text{m}}$  and  $N_i^{100\mu\text{m}}$  to the reader. This overall uncertainty is here considered to be typically better than about 50% (when considering the variability between all D14 campaigns). This value is now reported in Sec. 3.1 and A3 of the revised manuscript.

---

RC: The lead author gave a nice talk about this retrieval at the A-Train Symposium in 2017. Henceforth,  $N_i$  refers to  $N_i$  for ice particle maximum dimension  $D > 5\mu\text{m}$ . Slide 20 of this presentation, showing global distributions of  $N_i$  for  $10^\circ\text{C}$  intervals, appears almost identical to Fig. 9 of this paper for  $T < -30^\circ\text{C}$ , except that the  $N_i$  legends differ. The  $N_i$  values reported in the presentation are higher by a factor of about 1.7 relative to the  $N_i$  reported in Fig. 9 of this paper. What is the reason for this difference?

AR: We are grateful that the referee took the time to verify the consistency between this paper and the results presented during the A-Train Symposium. The figure referred to here (slide 20 of this presentation, available on <http://atrain2017.org>), corresponded to the  $N_i$  integrated from  $D_{\text{min}} = 1\mu\text{m}$ . This may not have been clearly expressed during the presentation but is suggested by the absence of mention to the size in the label. The  $1\mu\text{m}$  threshold was initially used at early stages of our analyses, but was subsequently changed to  $5\mu\text{m}$  as it is impossible at this point to reasonably evaluate DARDAR-LIM between 1 and  $5\mu\text{m}$ . Also, as discussed before, uncertainties related to PSD shape assumptions are likely to be even more important if  $D_{\text{min}} = 1\mu\text{m}$ .

Fig. 1 shown in this response corresponds to the distribution of  $N_i^{1\mu\text{m}}$  based on the dataset used for this paper. It can be noted that similar values to those shown during the A-Train Symposium presentation are found, despite small differences in absolute values. These could be due to an error found in the script that converts  $D_{\text{min}}$  from maximum diameter to an equivalent melted size prior to the numerical integration of the PSD, which led to slightly underestimated  $D_{\text{min}}$  and thus to higher concentration. This error was corrected before creating the dataset used in these papers. To the best of the first author's knowledge, there should be no other difference between Fig. 1 of this response and the figure in the A-Train Symposium presentation.

---

Major Comments

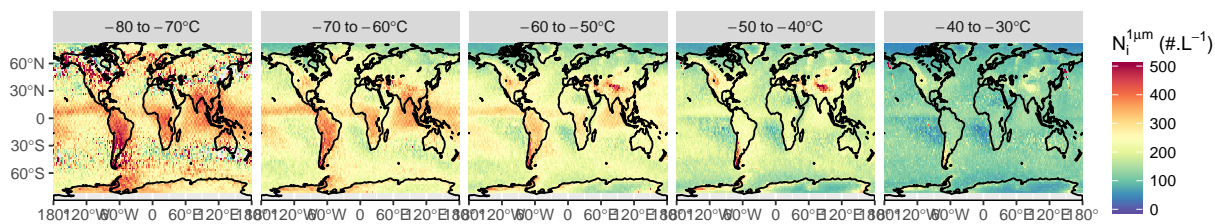


Figure 1: Spatial distribution of  $N_1^{1\mu m}$  from 2006 to 2016, averaged in a  $2 \times 2^\circ$  lat-lon grid and per  $10^\circ$  C temperature bin from  $-80$  to  $-30^\circ$  C.

1. RC: Page 8, line 25: The 2DS photodiode array length is  $1280 \mu\text{m}$ , which should be noted. Evidently the “time dimension” is used to size particles up to  $3205 \mu\text{m}$ ; please indicate the particle selection criteria used to size and count particles.

AR: We are very thankful to the referee for this comment that has led us to investigate in greater detail the various selection criteria for particle size and count that are available for the 2D-S instrument.

In the original manuscript, ATTREX-2014 data was processed with the method  $M_1$ , or  $M_7$  method when available. There are important differences between these methods, in particular concerning the size selection, which are for instance extensively described and discussed in Lawson [2011] and Erfani and Mitchell [2016]. The SPARTICUS data was treated with the  $M_1$  method only, as  $M_7$  isn’t operationally available in the ARM database. Comparing concentrations from these 2 methods should not be an issue as Erfani and Mitchell [2016] showed that the number concentration in small particle isn’t significantly different between them.

Nevertheless, after further discussion with the 2D-S data providers at SPEC Inc. (P. Lawson and S. Woods), it appeared that using a SPARTICUS dataset based on a  $M_4/M_1$  processing could be better adapted to the needs of this study. By  $M_4/M_1$  it is meant that the  $M_4$  method is used for particles sizes less than  $365 \mu\text{m}$  and the  $M_1$  is used otherwise. A main differences between these two methods is that  $M_4$  resizes out-of-focus particles to equivalent in-focus spheres [Korolev, 2007]. This becomes problematic when the ice particle shapes become strongly non-spherical, and this method can therefore only be applied to small particles. Consequently, it was decided with the SPARTICUS 2D-S data providers that a combined  $M_4/M_1$  processing method should be used here.

The differences between the PSDs obtained from  $M_1$  alone and  $M_4/M_1$  are shown in Fig. 2 of this document. The main difference occur for sizes between about  $30$  to  $100\text{--}200 \mu\text{m}$ , with typically more particles with  $D < 100 \mu\text{m}$  and less particles larger than this threshold. As a consequence, the bi-modal structure is less pronounced in  $M_4/M_1$ , but it also is clear from this figure that the results discussed in the original manuscript are not changed by this transition from  $M_1$  to  $M_4/M_1$  2D-S data. It can also be mentioned that slightly less flights with  $M_4/M_1$  treatments were available on the ARM database.

As a response to this comment, Sec. 3.2.1 was edited to explicitly mention the use of the  $M_n$  methods.

Regarding the photodiode specifications, it seems that the 2DS photodiode array length is (if referring to the actual physical size of the array) of about  $7.3 \text{ mm}$  [Lawson et al., 2006]. However, we fully agree with the referee that, because (i) the equivalent size of each photodiode

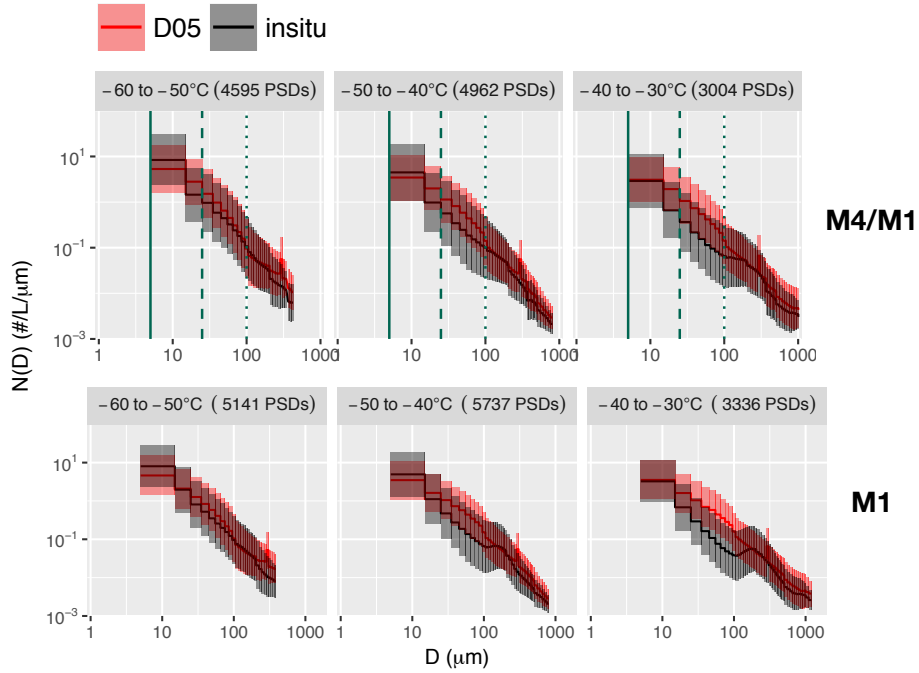


Figure 2: Comparison between the SPARTICUS 2D-S PSDs obtained from the M4/M1 (top; as in Fig. 1 of the revised manuscript) and the M1 method (bottom; as in Fig. 1 of original manuscript.)

is about  $10\ \mu\text{m}$  (considering the laser beam magnification) and (ii) the 2D-S being equipped with 128 photodiode, this instrument technically measures particules up to  $1280\ \mu\text{m}$  in size and so an extension to  $3205\ \mu\text{m}$  is only possible by using a time dimension (i.e., by using 2 consecutive measurements a of  $1280\ \mu\text{m}$  particle). This is now mentioned in Sec. 3.2.1 of the revised manuscript.

---

2. RC: Figure 5 and Sec. 4.2: For  $T > -50\text{C}$ , by what factor is  $N_i$  ( $D_{\min} = 5\ \mu\text{m}$ ) overestimated, on average? For  $T \geq -50\text{C}$ ?

AR: Based on Fig. 5 of the original manuscript, an overestimation of  $N_i^{5\ \mu\text{m}}$  by a factor of about 2 to 3 can be considered if looking at the distance between the modes of the 2D-S and DARDAR-LIM distributions. We nevertheless agree that this figure did not provide an easy way to clearly quantify the bias, and visually comparing the modes does not really provide a real statistical estimate of the differences between DARDAR-LIM and the 2D-S. This figure has therefore been edited in order to include the geometric means associated with each histogram (DARDAR-LIM, D05 and 2D-S) for each temperature bin and instrumental condition. These should allow for a more quantitative discussion of the biases, included in the revised Sec. 4.2. For instance, overestimations by about 10 to 30% and 20 to 60% are found in the mean values of  $N_i^{25\ \mu\text{m}}$  by D05 and DARDAR-LIM, respectively.

Complementarily, a line showing a factor of 3 around to one-to-one line has also been added to Fig. 4 of the original manuscript, now Fig. S4 of the complementary materials.

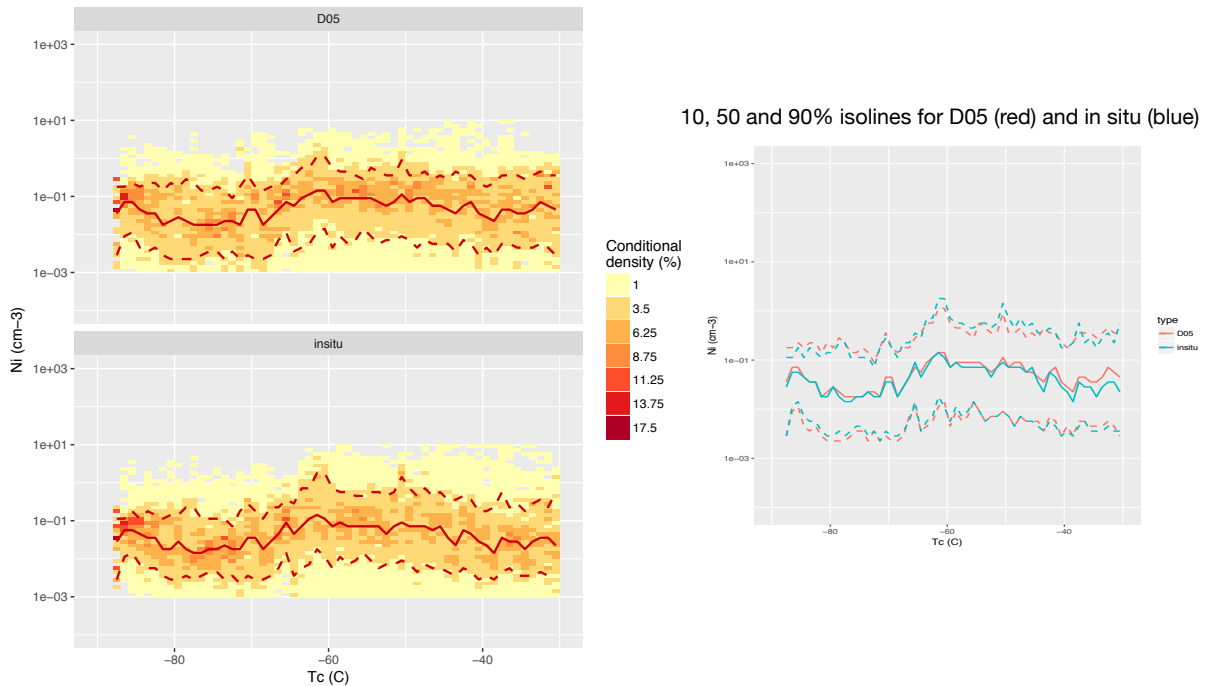


Figure 3: Left: Conditional density of  $N_i^{5\mu\text{m}}$  as function of the temperature, obtained from the insitu data used in this paper (bottom) and the corresponding D05 predictions (top). Plain red lines indicate the median and dashed lines show the 10th and 90th percentiles. The right panel directly compares the medians and 10th and 90th percentile lines.

3. RC: Page 21, lines 9-12: The strong temperature dependence of Ni mentioned here appears at variance with the in situ measurements reported in Krämer et al. (2009). Please mention this.

AR: We thank the referee for this comment, which has encouraged us to further compare our  $N_i$  products with the insitu findings in several studies by Krämer et al.

It should first be mentioned that it is very difficult to compare the temperature dependence of  $N_i$  obtained from in situ campaigns to those from global results shown in Sec. 6. In situ measurements are rather sparse and it is often difficult to tell what part of the cloud has been sampled. However, the enormous advantage of the dataset by Krämer et al is indeed that it consistently merges numerous in situ campaigns and should therefore tend to being comparable to global satellite data. This dataset is still being improved as airborne campaigns are continuously being added. The  $N_i(T)$  relation reported in Krämer et al. [2009] was based on a dataset that was not yet very large and contains some flights in mountain wave clouds that enhanced the frequencies of higher ice concentrations. A new, yet unpublished, dataset called JULIA does not confirm the (slight) dependence of Ni on T shown in Krämer et al. [2009]

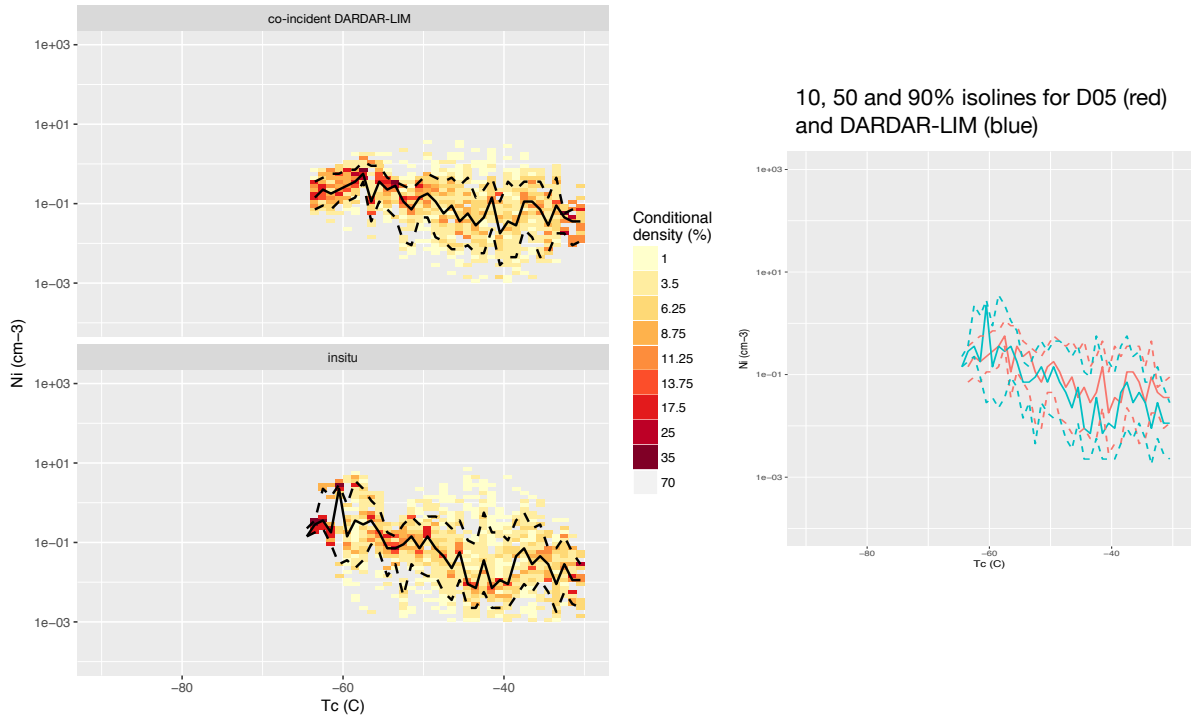


Figure 4: Same as 3 but for DARDAR-LIM  $N_i^{5\mu\text{m}}$  compared to co-incident in situ observations during SPARTICUS.

(personal communication, M. Krämer).

This comment has motivated us to compare the  $N_i(T)$  obtained in this study with the one from JULIA. Due to the complexity of this task, intermediate steps were taken. First, we have verified that the issues noted with D05 (notably due to its limited shape assumptions) does not create clear biases in the  $N_i(T)$  relation. This is shown in Fig. 3 attached to this response, which compares the  $N_i(T)$  dependency obtained from the dataset used in this study to that predicted by D05 based on the in situ data. It can be noted that the consistency of the relation found from our dataset to the one from JULIA has been verified, although this cannot be directly demonstrated here due to the latter being unpublished. Fig. 3 clearly shows that D05 is very well capable of reproducing the relation between  $N_i^{5\mu\text{m}}$  and  $T_c$  found in the in situ measurements, and so similar results could be expected from DARDAR. This has been verified by looking at the same relations based on the co-incident SPARTICUS flights. Fig. 4 in this response shows that DARDAR-LIM reproduces well the  $N_i(T)$  relation observed by the 2D-S. We have checked that these results also hold for  $N_i^{25\mu\text{m}}$  and that they are not sensitive to instrumental conditions.

Consequently, it could be expected that  $N_i(T)$  obtained from global DARDAR-LIM estimates are reasonable and that the observations from Sec. 6 are not necessarily at variance with in situ observations. However, the results presented here are preliminary and further analyses are necessary to confirm them. For instance, it would require to subset similar regions, cloud

type or distance from cloud top by comparison the in situ data. Rigorously assessing the consistency between  $N_i(T)$  observed from DARDAR-LIM and from in situ measurement would be extremely interesting but unfortunately out of the scope of this paper. These results will be the focus in a following study.

---

4. RC: Figure 9 and Sec. 6.1: For  $T > -50^\circ\text{C}$ ,  $N_i$  tends to be lower over regions characterized by extensive marine stratus, like off the west coasts of South America and Africa (from equator and southwards). Is this result real, or is it an artefact of the retrieval? If the latter is true, please explain.

AR: We thank the referee for pointing this out. It is correct that  $N_i$  (for all integration thresholds) tend to be relatively lower in marine stratocumulus regions. There does not seem to be any obvious reason to doubt the retrieval method in these regions but it should indeed be kept in mind that there are relatively less ice clouds in these subsidence regions. The spatial distributions of retrieval counts have now been added to supplementary materials (see Fig. S8) to help determining which regions correspond to statistically significant retrievals. Another physical explanation could be that there are no convective clouds in these regions, which seem to drive the high  $N_i^{5\mu\text{m}}$  and  $N_i^{25\mu\text{m}}$  observed in this figure. This is supported by the seasonal variabilities in  $N_i$  maps shown in Fig. 8 of the revised manuscript. Consequently, values observed correspond to thin cirrus, perhaps remnants of aged anvils or jet stream cirrus, and  $N_i^{5\mu\text{m}}$  values below  $100\text{L}^{-1}$  for  $T > -50^\circ\text{C}$  are thus not surprising, as mentioned in comment #7 of this review. It also means that  $N_i^{5\mu\text{m}}$  in this regions are more comparable to cloud-top values observed in the part 2 paper. This is now noted in Sec. 6.1 of the revised manuscript.

---

5. RC: Page 21, lines 14-19: A similar finding was reported in Mitchell et al. (2016, ACPD), where the highest  $N_i$  were associated with mountainous terrain. (Although this paper was rejected since the editor felt the retrieved  $N_i$  values were too high, and therefore could not be used to infer nucleation modes, no arguments cast doubt on the spatial and temporal relative differences in  $N_i$ , which still appear meaningful.)

AR: We fully agree that further comparisons to existing climatologies would be beneficial to the analyses in Sec. 6.1. A new paragraph discussing comparisons results by Mitchell et al. [2016, 2018] is now included.

---

6. RC: Page 22, lines 7-9: It is more meaningful to compare model results against observations than vice-versa. Suggest removing this paragraph. For example, in the modeling study by Zhou et al. (2016, ACP), the sensitivity of homo- and heterogeneous ice nucleation to various model parameters and updraft schemes were evaluated. Depending on how these are represented, one can get a broad range of  $N_i$ -temperature dependences, including  $N_i$  that is relatively insensitive to temperature (similar to the in situ observations of Krämer et al., 2009, ACP), and that modeling result would not support these DARDAR-LIM findings.

AR: We agree with this comment, comparisons to modeling would require further analyses that are not in the scope of this paper. This paragraph is now removed



---

7. RC: Figure 10 and Sec. 6.2:  $N_i$  ( $D_{\min}=5 \mu\text{m}$ ) in the tropics appears contrary to the  $N_i$  results in Fig. 1 and Fig. 5 of Part 2 of this study by Gryspeerdt et al. (submitted). Fig. 1a of Gryspeerdt et al. show  $N_i$  near cloud top while their Fig. 5 shows that  $N_i$  does not change appreciably with distance below cloud top (up to 3 km from cloud top) between  $-50$  and  $-60^\circ\text{C}$ . Assuming this result extends to other temperatures, the cloud top results in Fig. 1a of Gryspeerdt et al. should also be approximately valid below cloud top. Regarding Fig. 1a in Gryspeerdt et al., for  $T > -65^\circ\text{C}$ ,  $N_i$  is never higher in the tropics relative to the midlatitudes. Between  $-55$  and  $-40^\circ\text{C}$ , where the most optically thick cirrus clouds exist (cirrus defined as clouds having  $T < -38^\circ\text{C}$ ),  $N_i$  in the tropics is substantially lower than  $N_i$  in the midlatitudes. In Fig. 10 of Part 1 (Sourdeval et al.),  $N_i$  increases abruptly in the tropics for  $T < -40^\circ\text{C}$  (shown by the dashed curve), with  $N_i$  here being typically higher than  $N_i$  at similar  $T$  in the midlatitudes. This result appears opposite to the findings in Fig. 1a of Gryspeerdt et al. (Part 2). In addition, the CALIPSO  $N_i$  retrievals of Mitchell et al. (2016, ACPD) qualitatively support the findings of Gryspeerdt et al. (in terms of relative differences), and the in situ measurements from Mühlbauer et al. (2014) show relatively lower “peak  $N_i$ ” values in anvil cirrus (vs. frontal, jet stream and ridge-crest cirrus). Finally, several studies (e.g. Jensen et al., 2013, PNAS; Spichtinger and Krämer, 2013, ACP), show that tropical tropopause layer (TTL) cirrus tend to have  $N_i < 30 \text{L}^{-1}$ . Since the areal coverage of TTL cirrus exceeds that of anvil cirrus, and TTL cirrus tend to be higher than anvil cirrus (Gasparini et al., 2017, J. Climate), the  $N_i$  of  $\sim 200 \text{L}^{-1}$  in the TTL region in Fig. 10 appears at variance with in situ observations. Please comment on, and, if possible, reconcile these issues.

AR: We thank the referee for this interesting comment. It has motivated us to further compare the spatial distributions obtained from cloud-top  $N_i$  ( $N_{i(top)}$ ) (part 2) vs. the “all cloud” maps (part 1).

It is first important to point out that this is not straightforward as these two maps are not necessarily representative of the same cloud types within a given temperature bin. For instance, the  $N_{i(top)}$  map between  $-50$  and  $-60^\circ\text{C}$  (in part 2) only shows concentrations for clouds that have a cloud-top within this temperature bin, whereas the total  $N_i$  map (in part 1) also features values that are within deep convective clouds. It is observed that the high values of  $N_i^{5\mu\text{m}}$  and  $N_i^{25\mu\text{m}}$  only appear in convective regions, which is confirmed by the seasonal variabilities showed in Fig. 8. The sampling difference is also clear when comparing retrieval counts between  $N_{i(top)}$  and  $N_i$  per  $T_c$  bin, now showed in Fig. 1 of the revised part 2 paper and in Fig. S8 of the revised part 1 paper, respectively. Nearly no retrievals are present in the tropic for the  $N_{i(top)}$  map, whereas convective clouds are present in the  $N_i$  map. To support this analysis, it can be noted that high  $N_i$  values found between  $-50$  and  $-60^\circ\text{C}$  within deep convective clouds is in agreement with modeling results by Paukert et al. [2017], who also reports  $N_{i(top)}$  lower than  $N_i$  for this cloud type.

It could as well be argued that the CALIPSO  $N_i$  retrievals presented in Mitchell et al. [2016, 2018] are also more comparable to the  $N_{i(top)}$  map as the thermal infrared measurements used in these studies extinguishes within a few optical depth. It is therefore reasonable to expect that retrievals from these studies would not compare exactly to  $N_i$  maps presented in part 1 but more to the  $N_{i(top)}$  maps presented in part 2, as it is the case (in terms of relative variations of  $N_i$ ).

Regarding the absolute values of  $N_i$ , we completely agree with the referee that the ones



presented our maps may not be completely exact. An overestimation by a factor of 2, or even 3, could be expected on  $N_i^{5\mu\text{m}}$  considering all uncertainties on the retrievals (especially concerning the assumptions on the PSD shape). These uncertainties should be smaller on  $N_i^{25\mu\text{m}}$ , as the impact of the shape is less significant, and the spatial distributions of  $N_i^{25\mu\text{m}}$  are now also included in Fig. 7 of the revised manuscript. The relative variations are similar to those found for  $N_i^{5\mu\text{m}}$ , despite a slightly weaker temperature dependence, possibly due to the less directly link between particles with  $D > 25\mu\text{m}$  and homogeneous freezing processes. Maximum  $N_i^{25\mu\text{m}}$  (found at  $T_c < -70^\circ\text{C}$  in the tropics) are about  $100\text{L}^{-1}$ , which is more consistent with values found in the studies referred to here by the referee. Exact comparisons between our results and previous in situ findings would nevertheless require further investigation that are out of the scope of this study.

Sec. 6.1 has been substantially edited to include all the aforementioned discussions, and further explanations on the consistency between  $N_i$  and  $N_{i(top)}$  maps are now also given in the revised part 2 manuscript

---

8. RC: Page 23, lines 1-3 and Fig. 10: Fig. 10 and this text indicate that in the midlatitudes for  $T_i < -40\text{C}$ ,  $N_i$  is highest during winter and lowest during summer. This same result was found in Mitchell et al. (2016). One of the ACP review criteria questions is “Do the authors give proper credit to related work and clearly indicate their own new/original

AR: We agree that the consistency between our results and those of Mitchell et al. [2016], especially in the mid-latitude, should have been included. A paragraph is now dedicated to these comparisons in Sec. 6.1.

---

Minor comments

RC: 1. Page 15, line 9: much => slightly?

2. Page 19, line 6: follows => follow?

3. Page 22, line 13: at => as?

4. Figure 10 caption: Mention the meaning of the dashed curve.

5. Page 20, line 1: an => a?

AR: We thank the referee for pointing this out, these typos are corrected in the revised manuscript.

## References:

- J. Delanoë, A. J. Heymsfield, A. Protat, A. Bansemer, and R. J. Hogan. Normalized particle size distribution for remote sensing application. *J. Geophys. Res.*, 119(7):4204–4227, 2014. doi: 10.1002/2013JD020700. URL <http://dx.doi.org/10.1002/2013JD020700>.
- E. Erfani and D. L. Mitchell. Developing and bounding ice particle mass- and area-dimension expressions for use in atmospheric models and remote sensing. *Atmos. Chem. Phys.*, 16(7):4379–4400, 2016. doi: 10.5194/acp-16-4379-2016.
- A. Korolev. Reconstruction of the sizes of spherical particles from their shadow images. part i: Theoretical considerations. *J. Atmos. Oceanic Technol.*, 24(3):376–389, 2007. doi: 10.1175/JTECH1980.1.
- M. Krämer, C. Schiller, A. Afchine, R. Bauer, I. Gensch, A. Mangold, S. Schlicht, N. Spelten, N. Sitnikov, S. Borrmann, M. de Reus, and P. Spichtinger. Ice supersaturations and cirrus cloud crystal numbers. *Atmos. Chem. Phys.*, 9(11):3505–3522, 2009. doi: 10.5194/acp-9-3505-2009.
- R. P. Lawson. Effects of ice particles shattering on the 2d-s probe. *Atmos. Meas. Tech.*, 4(7):1361–1381, 2011. doi: 10.5194/amt-4-1361-2011. URL <http://www.atmos-meas-tech.net/4/1361/2011/>.
- R. P. Lawson, D. O’Connor, P. Zmarzly, K. Weaver, B. Baker, Q. Mo, and H. Jonsson. The 2D-S (Stereo) probe: Design and preliminary tests of a new airborne, high-speed, high-resolution particle imaging probe. *J. Atmos. Oceanic Technol.*, 23(11):1462–1477, 2006. doi: 10.1175/JTECH1927.1.
- D. L. Mitchell, A. Garnier, M. Avery, and E. Erfani. Calipso observations of the dependence of homo- and heterogeneous ice nucleation in cirrus clouds on latitude, season and surface condition. *Atmos. Chem. Phys. Discuss.*, 2016:1–60, 2016. doi: 10.5194/acp-2016-1062.
- D. L. Mitchell, A. Garnier, J. Pelon, and E. Erfani. Calipso (iir-caliop) retrievals of cirrus cloud ice particle concentrations. *Atmospheric Chemistry and Physics Discussions*, 2018:1–60, 2018. doi: 10.5194/acp-2018-526.
- M. Paukert, C. Hoose, and M. Simmel. Redistribution of ice nuclei between cloud and rain droplets: Parameterization and application to deep convective clouds. *J. Adv. Model. Earth Sy.*, 9(1):514–535, 2017. doi: 10.1002/2016MS000841.